Inclusive quarkonium photoproduction

Carlo Flore

Laboratoire de Physique des 2 Infinis
Irène Joliot-Curie (IJCLab), CNRS, Orsay

Quarkonia as Tools 2023
9 Jan 2023

Work done in collaboration with A. Colpani Serri, Y. Feng,
J.-P. Lansberg, M.A. Ozcelik, H.-S. Shao and Y. Yedelkina

This project is supported by the European Union's Horizon 2020 research and innovation programme under Grant agreement no. 824093

Inclusive quarkonium photoproduction

- We are looking at processes in which a near on-shell photon hits and breaks a proton to produce a quarkonium:

$$\gamma(Q^2 \sim 0) + p \to \mathcal{Q} + X$$

- treated in the Weizsäcker-Williams approximation
- extensively studied at HERA, relevant for the future EIC
- onium photoproduction achievable also in inclusive UPC reactions at the LHC

[see K. Lynch talk on Tuesday]

- resolved and diffractive contributions can be removed with cuts on elasticity $z = \frac{P_{\mathcal{Q}} \cdot P_p}{P_\gamma \cdot P_p}$
- feed-downs may be important and require dedicated studies

Quarkonium Production Model

Phys.Rept. 889 (2020) 1-106 & EPJC (2016) 76:107 for reviews

Quarkonium Production Model

Phys.Rept. 889 (2020) 1-106 & EPJC (2016) 76:107 for reviews

- A longstanding debate: not yet clear which mechanism is dominant

Quarkonium Production Model

Phys.Rept. 889 (2020) 1-106 & EPJC (2016) 76:107 for reviews

- A longstanding debate: not yet clear which mechanism is dominant
- Differences in the treatment of the hadronization

Quarkonium Production Model

Phys.Rept. 889 (2020) 1-106 & EPJC (2016) 76:107 for reviews

- A longstanding debate: not yet clear which mechanism is dominant
- Differences in the treatment of the hadronization
- 3 common models:

Quarkonium Production Model

Phys.Rept. 889 (2020) 1-106 & EPJC (2016) 76:107 for reviews

- A longstanding debate: not yet clear which mechanism is dominant
- Differences in the treatment of the hadronization
- 3 common models:
  1. COLOR SINGLET MODEL:
     hadronization w/o gluon emission; colour and spin are preserved during the hadronization

Quarkonium Production Model

Phys.Rept. 889 (2020) 1-106 & EPJC (2016) 76:107 for reviews

- A longstanding debate: not yet clear which mechanism is dominant
- Differences in the treatment of the hadronization
- 3 common models:
  1. Color Singlet Model:
     hadronization w/o gluon emission; colour and spin are preserved during the hadronization
  2. NRQCD and Color Octet Mechanism:
     higher Fock states of the mesons taken into account; $Q\bar{Q}$ can be produced in octet states with different quantum number as the meson;

Quarkonium Production Model

Phys.Rept. 889 (2020) 1-106 & EPJC (2016) 76:107 for reviews

- A longstanding debate: not yet clear which mechanism is dominant
- Differences in the treatment of the hadronization
- 3 common models:

1. COLOR SINGLET MODEL:
   hadronization w/o gluon emission; colour and spin are preserved during the hadronization
2. NRQCD AND COLOR OCTET MECHANISM:
   higher Fock states of the mesons taken into account; $Q\bar{Q}$ can be produced in octet states with different quantum number as the meson;
3. COLOR EVAPORATION MODEL:
   based on quark-hadron duality;
   only the invariant mass matters; semi-soft gluons emissions;
   color-wise decorrelated $c\bar{c}$ prod. and hadr.

Leading P_T approximation of NLO $J/\psi + g$: NLO*

P. Artoisenet *et al.*, PRL 101 (2008) 152001, J.-P. Lansberg, EPJC 61 (2009) 693 & PLB 679 (2009) 340

Leading P_T approximation of NLO $J/\psi + g$: NLO*

P. Artoisenet *et al.*, PRL 101 (2008) 152001, J.-P. Lansberg, EPJC 61 (2009) 693 & PLB 679 (2009) 340

- NLO* only contains the real-emission contributions with an IR cut-off, $\sqrt{s_{ij}^{\min}}$, and is expected to account for the leading P_T contributions at NLO (P_T^{-6})

Leading P_T approximation of NLO $J/\psi + g$: NLO*

P. Artoisenet *et al.*, PRL 101 (2008) 152001, J.-P. Lansberg, EPJC 61 (2009) 693 & PLB 679 (2009) 340

- NLO* only contains the real-emission contributions with an IR cut-off, $\sqrt{s_{ij}^{\min}}$, and is expected to account for the leading P_T contributions at NLO (P_T^{-6})
- Succesfully checked against full NLO computations for $P_T > 3$ GeV

Leading P_T approximation of NLO $J/\psi + g$: NLO*

P. Artoisenet *et al.*, **PRL 101 (2008) 152001, J.-P. Lansberg, EPJC 61 (2009) 693 & PLB 679 (2009) 340**

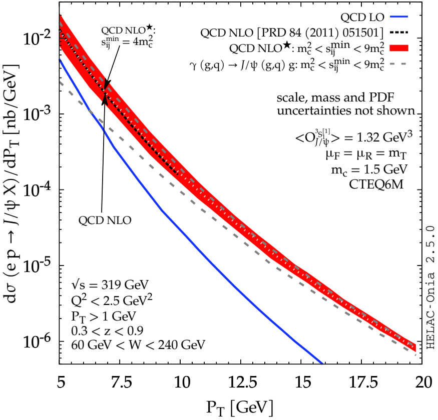

- NLO* only contains the real-emission contributions with an IR cut-off, $\sqrt{s_{ij}^{min}}$, and is expected to account for the leading P_T contributions at NLO (P_T^{-6})
- Succesfully checked against full NLO computations for $P_T > 3$ GeV

CSM QCD NLO from **PRD 84 (2011) 051501**

Leading P_T approximation of NLO $J/\psi + g$: NLO*

P. Artoisenet *et al.*, PRL 101 (2008) 152001, J.-P. Lansberg, EPJC 61 (2009) 693 & PLB 679 (2009) 340

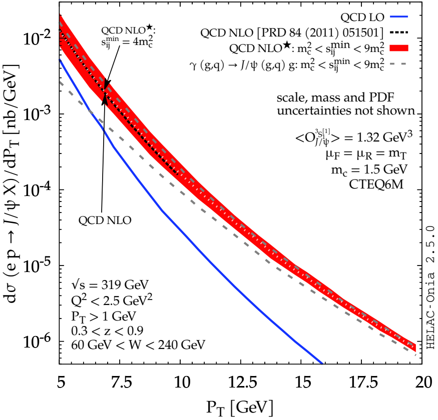

- NLO* only contains the real-emission contributions with an IR cut-off, $\sqrt{s_{ij}^{\min}}$, and is expected to account for the leading P_T contributions at NLO (P_T^{-6})
- Succesfully checked against full NLO computations for $P_T > 3$ GeV
- $\sqrt{s_{ij}^{\min}}/m_c \in [1:3]$ suitable for our study; $\sqrt{s_{ij}^{\min}} = 2m_c$ remarkably reproduces NLO results

CSM QCD NLO from **PRD 84 (2011) 051501**

Leading P_T approximation of NLO $J/\psi + g$: NLO*

P. Artoisenet *et al.*, PRL 101 (2008) 152001, J.-P. Lansberg, EPJC 61 (2009) 693 & PLB 679 (2009) 340

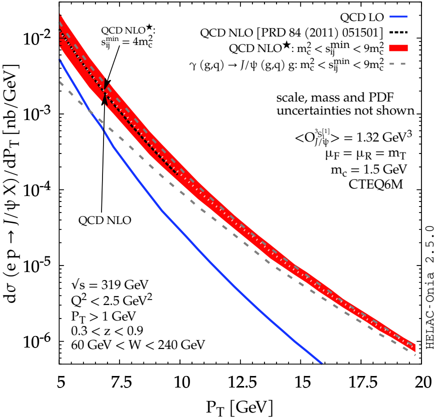

CSM QCD NLO from **PRD 84 (2011) 051501**

- NLO* only contains the real-emission contributions with an IR cut-off, $\sqrt{s_{ij}^{\min}}$, and is expected to account for the leading P_T contributions at NLO (P_T^{-6})
- Succesfully checked against full NLO computations for $P_T > 3$ GeV
- $\sqrt{s_{ij}^{\min}}/m_c \in [1:3]$ suitable for our study; $\sqrt{s_{ij}^{\min}} = 2m_c$ remarkably reproduces NLO results

Let's revisit HERA data!

Revisiting HERA data (I)

CF, J.-P. Lansberg, H.-S. Shao, Y. Yedelkina, PLB 811 (2020) 135926

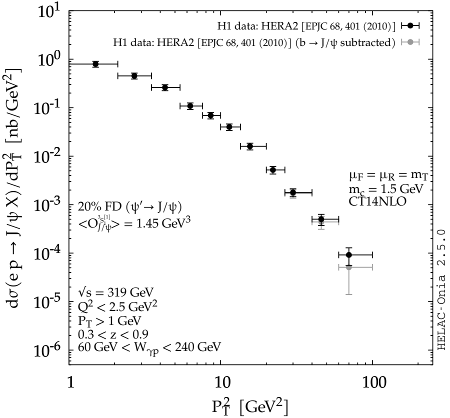

All the computations are done with HELAC-Onia [H.-S. Shao, CPC198 (2016) 238]. See also `https://nloaccess.in2p3.fr`

Revisiting HERA data (I)

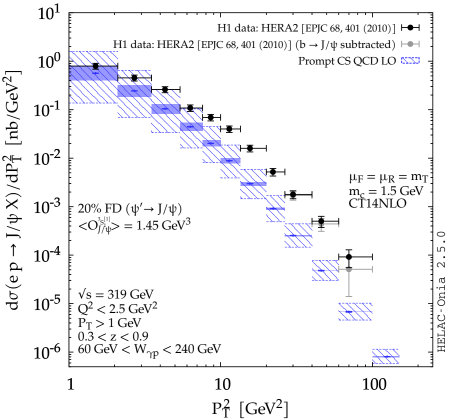

CF, J.-P. Lansberg, H.-S. Shao, Y. Yedelkina, PLB 811 (2020) 135926

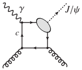

$\gamma + g \to \psi + g \; @ \; \alpha\alpha_s^2$

All the computations are done with HELAC-ONIA **[H.-S. Shao, CPC198 (2016) 238]**. See also `https://nloaccess.in2p3.fr`
Scale and mass uncertainties are shown by the hatched and solid bands respectively.

[The quark and antiquark attached to the ellipsis are taken as on-shell and their relative velocity v is set to zero.]

Revisiting HERA data (I)

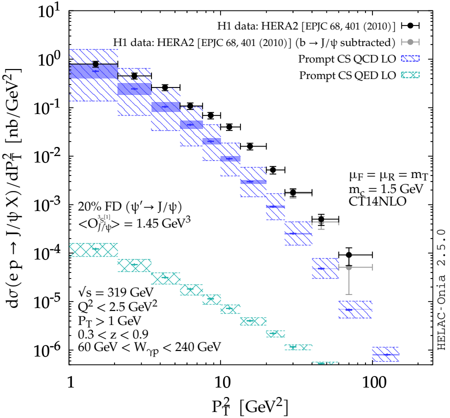

CF, J.-P. Lansberg, H.-S. Shao, Y. Yedelkina, PLB 811 (2020) 135926

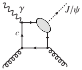

$\gamma + g \to \psi + g \ @ \ \alpha\alpha_s^2$

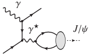

$\gamma + q \to \psi + q \ @ \ \alpha^3$ [NEW!]

All the computations are done with HELAC-ONIA [H.-S. Shao, CPC198 (2016) 238]. See also `https://nloaccess.in2p3.fr`
Scale and mass uncertainties are shown by the hatched and solid bands respectively.

[The quark and antiquark attached to the ellipsis are taken as on-shell and their relative velocity v is set to zero.]

Revisiting HERA data (I)

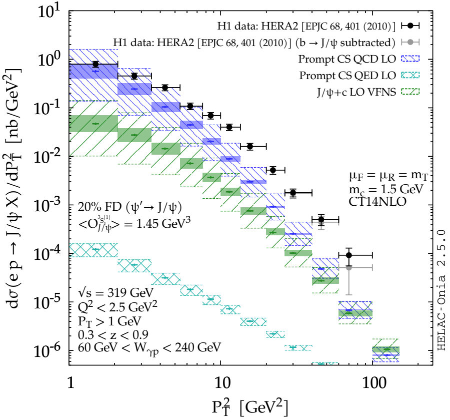

CF, J.-P. Lansberg, H.-S. Shao, Y. Yedelkina, PLB 811 (2020) 135926

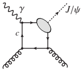

$\gamma + g \to \psi + g$ @ $\alpha\alpha_s^2$

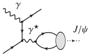

$\gamma + q \to \psi + q$ @ α^3 [NEW!]

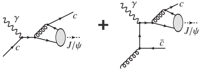

$$\left\{ \begin{array}{ll} \gamma+c\to\psi+c \text{ @ } \alpha\alpha_s^2 & \text{(4FS)} \\ \gamma+g\to\psi+c+\bar{c} \text{ @ } \alpha\alpha_s^3 & \text{(3FS)} \end{array} \right.$$ [also NEW!]

All the computations are done with HELAC-Onia [H.-S. Shao, CPC198 (2016) 238]. See also `https://nloaccess.in2p3.fr`
Scale and mass uncertainties are shown by the hatched and solid bands respectively.

[The quark and antiquark attached to the ellipsis are taken as on-shell and their relative velocity *v* is set to zero.]

Revisiting HERA data (I)

CF, J.-P. Lansberg, H.-S. Shao, Y. Yedelkina, PLB 811 (2020) 135926

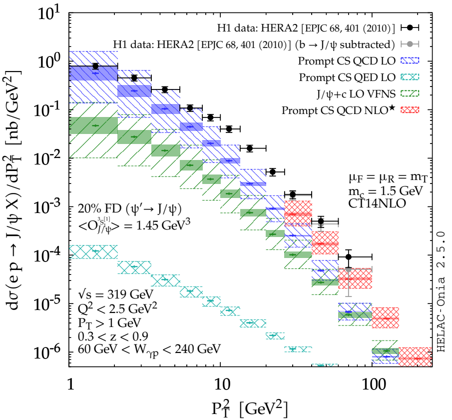

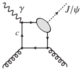

$\gamma + g \to \psi + g$ @ $\alpha\alpha_s^2$

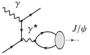

$\gamma + q \to \psi + q$ @ α^3 [NEW!]

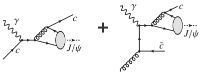

$\left\{ \begin{array}{ll} \gamma + c \to \psi + c \text{ @ } \alpha\alpha_s^2 & \text{(4FS)} \\ \gamma + g \to \psi + c + \bar{c} \text{ @ } \alpha\alpha_s^3 & \text{(3FS)} \end{array} \right.$ [also NEW!]

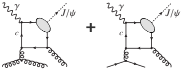

$\left\{ \begin{array}{l} \gamma + g \to \psi + g + g \text{ @ } \alpha\alpha_s^3 \\ \gamma + q \to \psi + g + q \text{ @ } \alpha\alpha_s^3 \end{array} \right.$

[+ $\gamma + g \to \psi + g$]

All the computations are done with HELAC-ONIA [H.-S. Shao, CPC198 (2016) 238]. See also `https://nloaccess.in2p3.fr`
Scale and mass uncertainties are shown by the hatched and solid bands respectively.

[The quark and antiquark attached to the ellipsis are taken as on-shell and their relative velocity *v* is set to zero.]

Revisiting HERA data (I)

CF, J.-P. Lansberg, H.-S. Shao, Y. Yedelkina, PLB 811 (2020) 135926

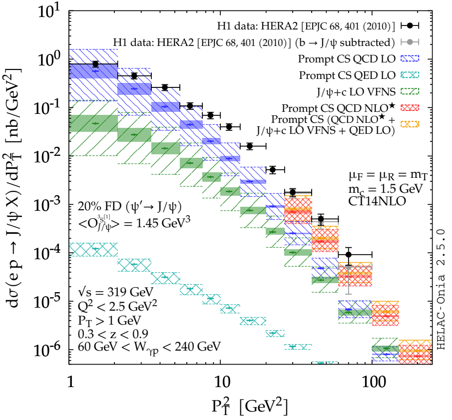

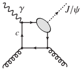

$\gamma + g \to \psi + g$ @ $\alpha\alpha_s^2$

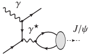

$\gamma + q \to \psi + q$ @ α^3 [NEW!]

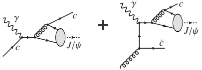

$$\left\{\begin{array}{ll} \gamma+c\to\psi+c \text{ @ } \alpha\alpha_s^2 & \text{(4FS)} \\ \gamma+g\to\psi+c+\bar{c} \text{ @ } \alpha\alpha_s^3 & \text{(3FS)} \end{array}\right.$$ [also NEW!]

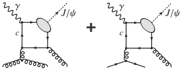

$$\left\{\begin{array}{l} \gamma+g\to\psi+g+g \text{ @ } \alpha\alpha_s^3 \\ \gamma+q\to\psi+g+q \text{ @ } \alpha\alpha_s^3 \end{array}\right.$$

[+ $\gamma + g \to \psi + g$]

All the computations are done with HELAC-Onia [H.-S. Shao, CPC198 (2016) 238]. See also `https://nloaccess.in2p3.fr`
Scale and mass uncertainties are shown by the hatched and solid bands respectively.

[The quark and antiquark attached to the ellipsis are taken as on-shell and their relative velocity *v* is set to zero.]

Revisiting HERA data (II)

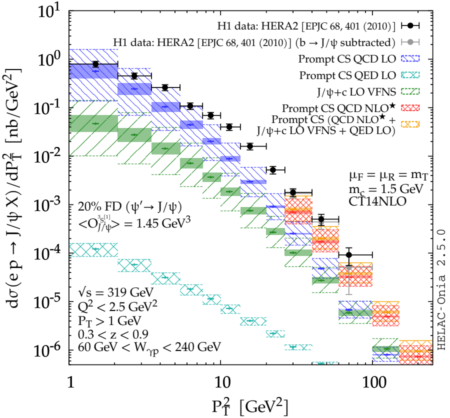

CF, J.-P. Lansberg, H.-S. Shao, Y. Yedelkina, PLB 811 (2020) 135926

- LO QCD works well at low P_T

Revisiting HERA data (II)

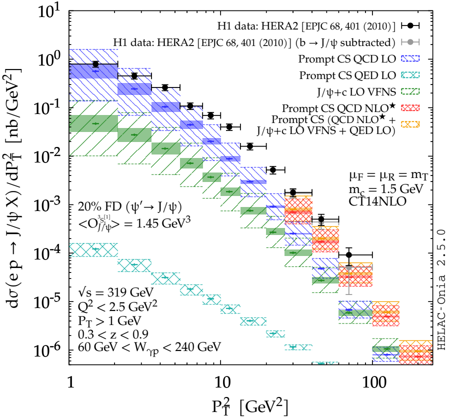

CF, J.-P. Lansberg, H.-S. Shao, Y. Yedelkina, PLB 811 (2020) 135926

- LO QCD works well at low P_T
- LO QED small, but much harder spectrum

Revisiting HERA data (II)

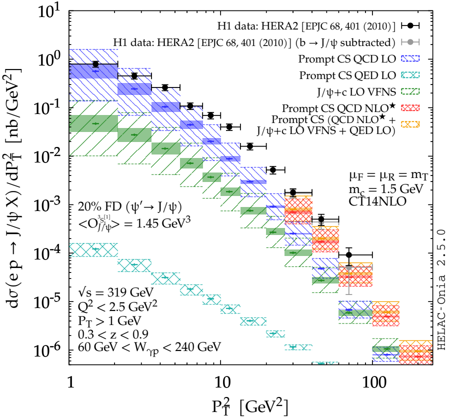

CF, J.-P. Lansberg, H.-S. Shao, Y. Yedelkina, PLB 811 (2020) 135926

- LO QCD works well at low P_T
- LO QED small, but much harder spectrum
- J/ψ+charm matters at large P_T

Revisiting HERA data (II)

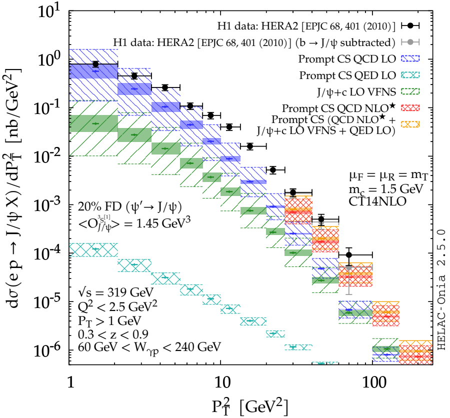

CF, J.-P. Lansberg, H.-S. Shao, Y. Yedelkina, PLB 811 (2020) 135926

- LO QCD works well at low P_T
- LO QED small, but much harder spectrum
- $J/\psi+$charm matters at large P_T
- NLO$^{(\star)}$ close to the data, the overall sum nearly agrees with them

Revisiting HERA data (II)

CF, J.-P. Lansberg, H.-S. Shao, Y. Yedelkina, PLB 811 (2020) 135926

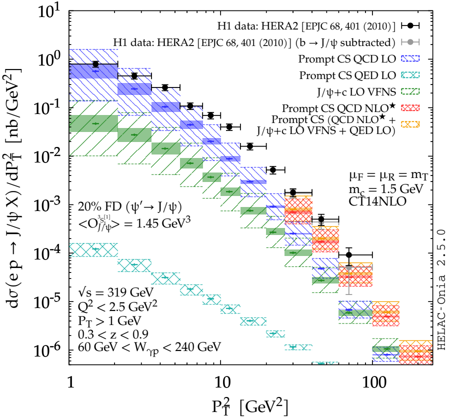

- LO QCD works well at low P_T
- LO QED small, but much harder spectrum
- J/ψ+charm matters at large P_T
- NLO$^{(\star)}$ close to the data, the overall sum nearly agrees with them
- Agreement with the last bin when the expected $b \to J/\psi$ feed down A (in gray) is subtracted

Revisiting HERA data (II)

CF, J.-P. Lansberg, H.-S. Shao, Y. Yedelkina, PLB 811 (2020) 135926

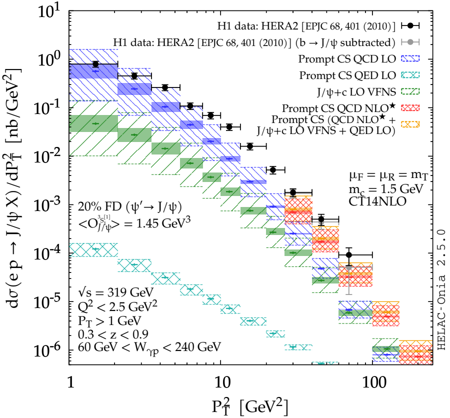

- LO QCD works well at low P_T
- LO QED small, but much harder spectrum
- J/ψ+charm matters at large P_T
- NLO$^{(\star)}$ close to the data, the overall sum nearly agrees with them
- Agreement with the last bin when the expected $b \to J/\psi$ feed down A (in gray) is subtracted

The CSM up to $\alpha\alpha_s^3$ reproduces J/ψ photoproduction at HERA

$\rightarrow$ we will restrict to CSM for our EIC predictions

$b \to J/\psi$ feed-down at HERA

J.-P. Lansberg, Phys.Rept. 889 (2020) 1-106;
CF, J.-P. Lansberg, H.-S. Shao, Y. Yedelkina, PLB 811 (2020) 135926

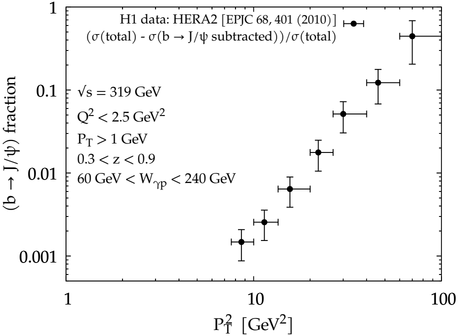

- $b \to J/\psi$ feed-down estimated from $b\bar{b}$ production data from H1 [EPJC 72 (2012) 2148]
- fraction of J/ψ from b over 40% for $P_T \lesssim 10$ GeV
- may become important also at the EIC at $\sqrt{s_{ep}} = 140$ GeV

$J/\psi + X$ at the EIC

$\left[\sqrt{s_{ep}} = 45 \text{ GeV}\right]$

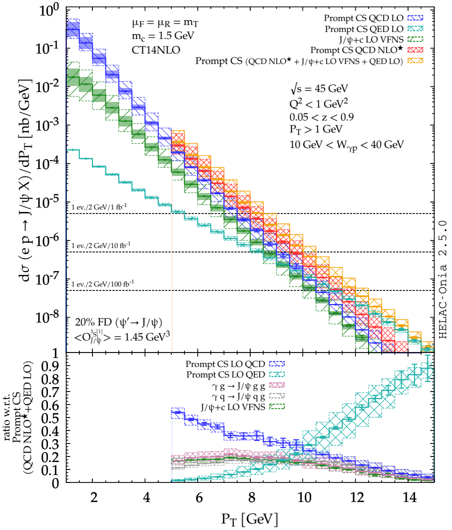

CF, J.-P. Lansberg, H.-S. Shao, Y. Yedelkina, PLB 811 (2020) 135926

- At $\sqrt{s_{ep}} = 45$ GeV, one gets into valence region

$J/\psi + X$ at the EIC

$[\sqrt{s_{ep}} = 45$ GeV$]$

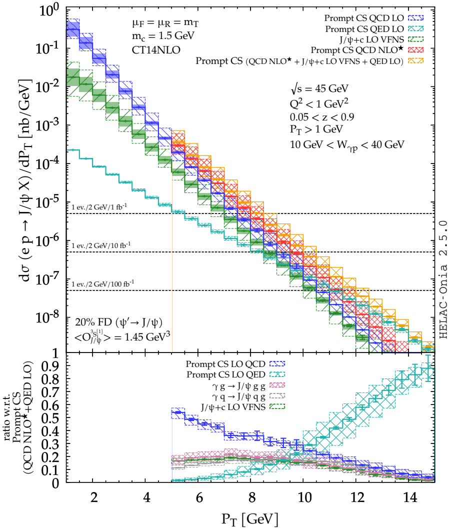

CF, J.-P. Lansberg, H.-S. Shao, Y. Yedelkina, PLB 811 (2020) 135926

- At $\sqrt{s_{ep}} = 45$ GeV, one gets into valence region
- Yield steeply falling with P_T
- Yield can be measured up to $P_T \sim 11$ GeV with $\mathcal{L} = 100$ fb^{-1}

[using both *ee* and $\mu\mu$ decay channels and $\varepsilon_{J/\psi} \simeq 80\%$]

$J/\psi + X$ at the EIC

$\left[\sqrt{s_{ep}} = 45 \text{ GeV}\right]$

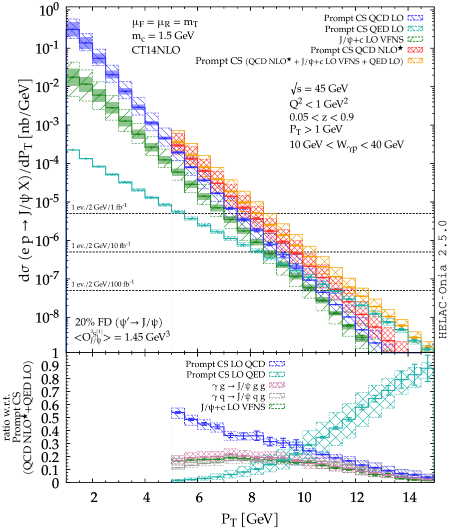

CF, J.-P. Lansberg, H.-S. Shao, Y. Yedelkina, PLB 811 (2020) 135926

- At $\sqrt{s_{ep}} = 45$ GeV, one gets into valence region
- Yield steeply falling with P_T
- Yield can be measured up to $P_T \sim 11$ GeV with $\mathcal{L} = 100$ fb^{-1}

  [using both ee and $\mu\mu$ decay channels and $\varepsilon_{J/\psi} \simeq 80\%$]
- QED contribution leading at the largest reachable P_T
- $\gamma + q$ fusion contributes more than 30% for $P_T > 8$ GeV

$J/\psi + X$ at the EIC

$\left[\sqrt{s_{ep}} = 140\ \text{GeV}\right]$

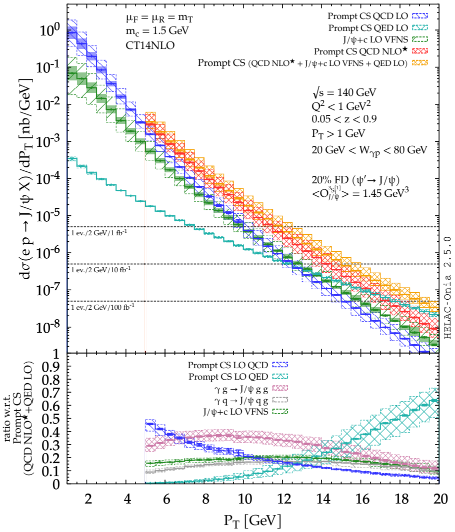

CF, J.-P. Lansberg, H.-S. Shao, Y. Yedelkina, PLB 811 (2020) 135926

- At $\sqrt{s_{ep}} = 140$ GeV larger P_T range, up to ~ 18 GeV

$J/\psi + X$ at the EIC

$[\sqrt{s_{ep}} = 140 \text{ GeV}]$

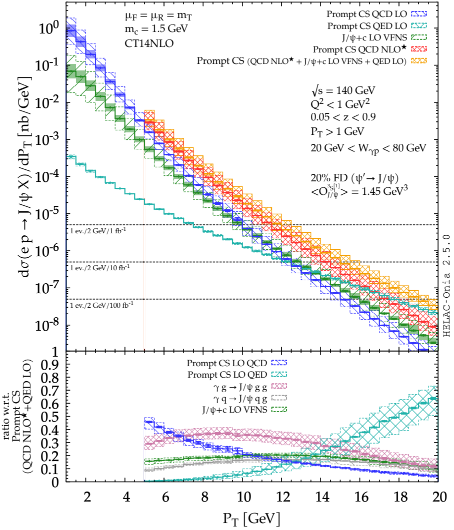

CF, J.-P. Lansberg, H.-S. Shao, Y. Yedelkina, PLB 811 (2020) 135926

- At $\sqrt{s_{ep}} = 140$ GeV larger P_T range, up to ~ 18 GeV
- QED contribution also leading at the largest reachable P_T
- $\gamma + g$ fusion contributions dominant up to $P_T \sim 15$ GeV

$J/\psi + X$ at the EIC

$\left[\sqrt{s_{ep}} = 140 \text{ GeV}\right]$

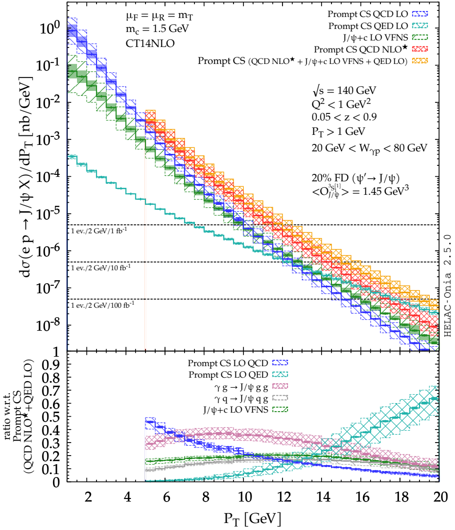

CF, J.-P. Lansberg, H.-S. Shao, Y. Yedelkina, PLB 811 (2020) 135926

- At $\sqrt{s_{ep}} = 140$ GeV larger P_T range, up to ~ 18 GeV
- QED contribution also leading at the largest reachable P_T
- $\gamma + g$ fusion contributions dominant up to $P_T \sim 15$ GeV
- $J/\psi + 2$ hard partons [*i.e.* $J/\psi + \{gg, qg, c\bar{c}\}$] dominant for $P_T \sim 8 - 15$ GeV

$J/\psi + X$ at the EIC

$[\sqrt{s_{ep}} = 140\ \text{GeV}]$

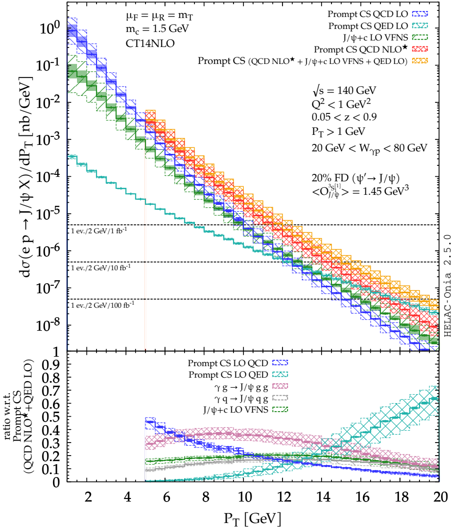

CF, J.-P. Lansberg, H.-S. Shao, Y. Yedelkina, PLB 811 (2020) 135926

- At $\sqrt{s_{ep}} = 140$ GeV larger P_T range, up to ~ 18 GeV
- QED contribution also leading at the largest reachable P_T
- $\gamma + g$ fusion contributions dominant up to $P_T \sim 15$ GeV
- $J/\psi + 2$ hard partons [*i.e.* $J/\psi + \{gg, qg, c\bar{c}\}$] dominant for $P_T \sim 8 - 15$ GeV
- It could lead to the observation of $J/\psi + 2$ jets with moderate P_T^{jet}

J/ψ+charm associated production at the EIC

CF, J.-P. Lansberg, H.-S. Shao, Y. Yedelkina, PLB 811 (2020) 135926

$J/\psi+$charm associated production at the EIC

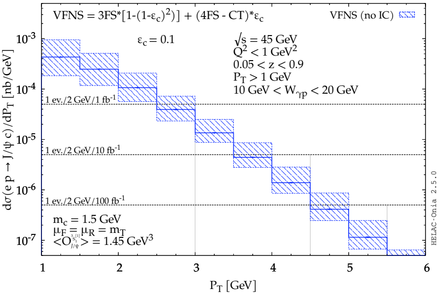

CF, J.-P. Lansberg, H.-S. Shao, Y. Yedelkina, PLB 811 (2020) 135926

- Same LO VFNS computation previously shown in green except for the charm-detection efficiency ε_c:

$$d\sigma^{\text{VFNS}} = d\sigma^{\text{3FS}}\left[1-(1-\varepsilon_c)^2\right] + \left(d\sigma^{\text{4FS}} - d\sigma^{\text{CT}}\right)\varepsilon_c$$

- At $\sqrt{s_{ep}} = 45$ GeV, yield limited to low P_T even with $\mathcal{L} = 100$ fb^{-1}
- But it is clearly observable if $\varepsilon_c = 0.1$ with $\mathcal{O}(500, 50, 5)$ events for $\mathcal{L} = (100, 10, 1)$ fb^{-1}

$J/\psi+$charm associated production at the EIC

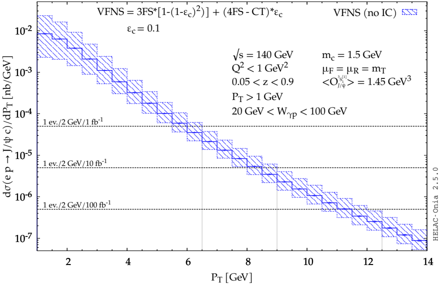

CF, J.-P. Lansberg, H.-S. Shao, Y. Yedelkina, PLB 811 (2020) 135926

- Same LO VFNS computation previously shown in green except for the charm-detection efficiency ε_c:

$$d\sigma^{\text{VFNS}} = d\sigma^{\text{3FS}}\left[1-(1-\varepsilon_c)^2\right] + \left(d\sigma^{\text{4FS}} - d\sigma^{\text{CT}}\right)\varepsilon_c$$

- At $\sqrt{s_{ep}} = 45$ GeV, yield limited to low P_T even with $\mathcal{L} = 100$ fb^{-1}
- But it is clearly observable if $\varepsilon_c = 0.1$ with $\mathcal{O}(500, 50, 5)$ events for $\mathcal{L} = (100, 10, 1)$ fb^{-1}
- At $\sqrt{s_{ep}} = 140$ GeV, P_T range up to 10 GeV with up to thousands of events with $\mathcal{L} = 100$ fb^{-1}
- Could be observed via charm jet

J/ψ+charm associated production at the EIC

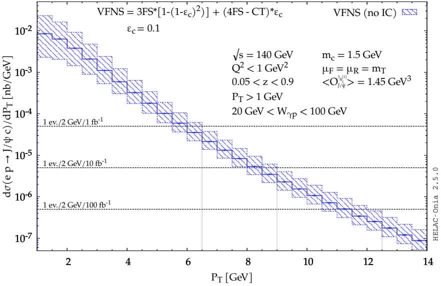

CF, J.-P. Lansberg, H.-S. Shao, Y. Yedelkina, PLB 811 (2020) 135926

- Same LO VFNS computation previously shown in green except for the charm-detection efficiency ε_c:

$$d\sigma^{\text{VFNS}} = d\sigma^{\text{3FS}}\left[1-(1-\varepsilon_c)^2\right] + \left(d\sigma^{\text{4FS}} - d\sigma^{\text{CT}}\right)\varepsilon_c$$

- At $\sqrt{s_{ep}} = 45$ GeV, yield limited to low P_T even with $\mathcal{L} = 100$ fb^{-1}
- But it is clearly observable if $\varepsilon_c = 0.1$ with $\mathcal{O}(500, 50, 5)$ events for $\mathcal{L} = (100, 10, 1)$ fb^{-1}
- At $\sqrt{s_{ep}} = 140$ GeV, P_T range up to 10 GeV with up to thousands of events with $\mathcal{L} = 100$ fb^{-1}
- Could be observed via charm jet

- 4FS $\gamma c \to J/\psi c$ depends on $c(x)$ and could be enhanced by intrinsic charm

$J/\psi+$charm associated production at the EIC

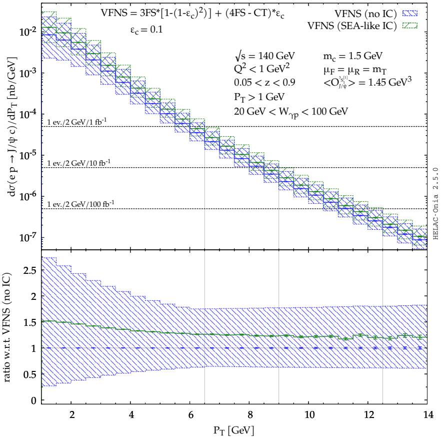

CF, J.-P. Lansberg, H.-S. Shao, Y. Yedelkina, PLB 811 (2020) 135926

- Same LO VFNS computation previously shown in green except for the charm-detection efficiency ε_c:

$$d\sigma^{\mathrm{VFNS}} = d\sigma^{\mathrm{3FS}}\left[1-(1-\varepsilon_c)^2\right] + \left(d\sigma^{\mathrm{4FS}} - d\sigma^{\mathrm{CT}}\right)\varepsilon_c$$

- At $\sqrt{s_{ep}} = 45$ GeV, yield limited to low P_T even with $\mathcal{L} = 100$ fb^{-1}
- But it is clearly observable if $\varepsilon_c = 0.1$ with $\mathcal{O}(500, 50, 5)$ events for $\mathcal{L} = (100, 10, 1)$ fb^{-1}
- At $\sqrt{s_{ep}} = 140$ GeV, P_T range up to 10 GeV with up to thousands of events with $\mathcal{L} = 100$ fb^{-1}
- Could be observed via charm jet

- 4FS $\gamma c \to J/\psi c$ depends on $c(x)$ and could be enhanced by intrinsic charm
- Small effect at $\sqrt{s_{ep}} = 140$ GeV [We used IC $c(x)$ encoded in CT14NNLO]

$J/\psi+$charm associated production at the EIC

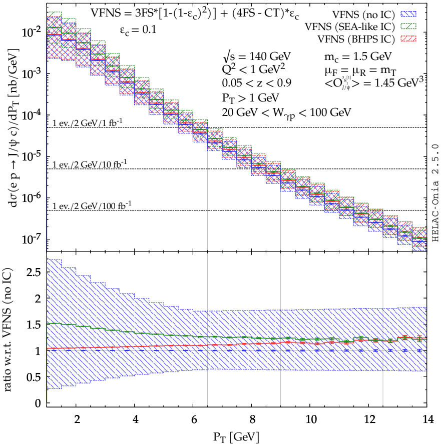

CF, J.-P. Lansberg, H.-S. Shao, Y. Yedelkina, PLB 811 (2020) 135926

- Same LO VFNS computation previously shown in green except for the charm-detection efficiency ε_c:

$$d\sigma^{\text{VFNS}} = d\sigma^{\text{3FS}}\left[1-(1-\varepsilon_c)^2\right] + \left(d\sigma^{\text{4FS}} - d\sigma^{\text{CT}}\right)\varepsilon_c$$

- At $\sqrt{s_{ep}} = 45$ GeV, yield limited to low P_T even with $\mathcal{L} = 100$ fb^{-1}
- But it is clearly observable if $\varepsilon_c = 0.1$ with $\mathcal{O}(500, 50, 5)$ events for $\mathcal{L} = (100, 10, 1)$ fb^{-1}
- At $\sqrt{s_{ep}} = 140$ GeV, P_T range up to 10 GeV with up to thousands of events with $\mathcal{L} = 100$ fb^{-1}
- Could be observed via charm jet

- 4FS $\gamma c \to J/\psi c$ depends on $c(x)$ and could be enhanced by intrinsic charm
- Small effect at $\sqrt{s_{ep}} = 140$ GeV [We used IC $c(x)$ encoded in CT14NNLO]

$J/\psi+$charm associated production at the EIC

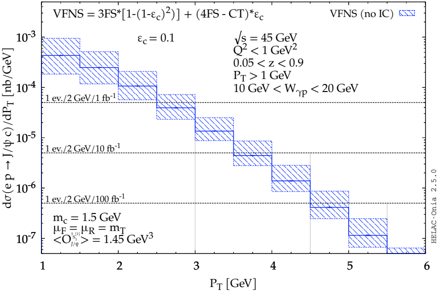

CF, J.-P. Lansberg, H.-S. Shao, Y. Yedelkina, PLB 811 (2020) 135926

- Same LO VFNS computation previously shown in green except for the charm-detection efficiency ε_c:

$$d\sigma^{\rm VFNS} = d\sigma^{\rm 3FS}\left[1-(1-\varepsilon_c)^2\right] + \left(d\sigma^{\rm 4FS} - d\sigma^{\rm CT}\right)\varepsilon_c$$

- At $\sqrt{s_{ep}} = 45$ GeV, yield limited to low P_T even with $\mathcal{L} = 100$ fb^{-1}
- But it is clearly observable if $\varepsilon_c = 0.1$ with $\mathcal{O}(500, 50, 5)$ events for $\mathcal{L} = (100, 10, 1)$ fb^{-1}
- At $\sqrt{s_{ep}} = 140$ GeV, P_T range up to 10 GeV with up to thousands of events with $\mathcal{L} = 100$ fb^{-1}
- Could be observed via charm jet

- 4FS $\gamma c \to J/\psi c$ depends on $c(x)$ and could be enhanced by intrinsic charm
- Small effect at $\sqrt{s_{ep}} = 140$ GeV [We used IC $c(x)$ encoded in CT14NNLO]
- Measurable effect at $\sqrt{s_{ep}} = 45$ GeV

$J/\psi+$charm associated production at the EIC

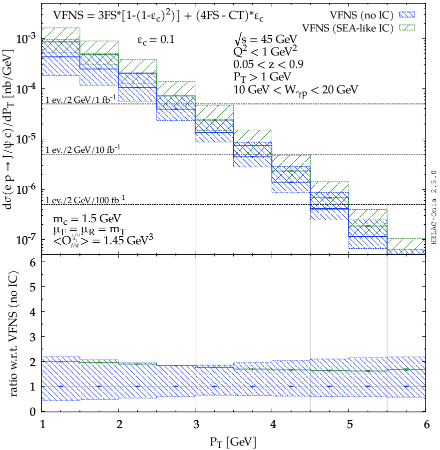

CF, J.-P. Lansberg, H.-S. Shao, Y. Yedelkina, PLB 811 (2020) 135926

- Same LO VFNS computation previously shown in green except for the charm-detection efficiency ε_c:

$$d\sigma^{\mathrm{VFNS}} = d\sigma^{\mathrm{3FS}}\left[1-(1-\varepsilon_c)^2\right] + \left(d\sigma^{\mathrm{4FS}} - d\sigma^{\mathrm{CT}}\right)\varepsilon_c$$

- At $\sqrt{s_{ep}} = 45$ GeV, yield limited to low P_T even with $\mathcal{L} = 100$ fb^{-1}
- But it is clearly observable if $\varepsilon_c = 0.1$ with $\mathcal{O}(500, 50, 5)$ events for $\mathcal{L} = (100, 10, 1)$ fb^{-1}
- At $\sqrt{s_{ep}} = 140$ GeV, P_T range up to 10 GeV with up to thousands of events with $\mathcal{L} = 100$ fb^{-1}
- Could be observed via charm jet

- 4FS $\gamma c \to J/\psi c$ depends on $c(x)$ and could be enhanced by intrinsic charm
- Small effect at $\sqrt{s_{ep}} = 140$ GeV

[We used IC $c(x)$ encoded in CT14NNLO]

- Measurable effect at $\sqrt{s_{ep}} = 45$ GeV

J/ψ+charm associated production at the EIC

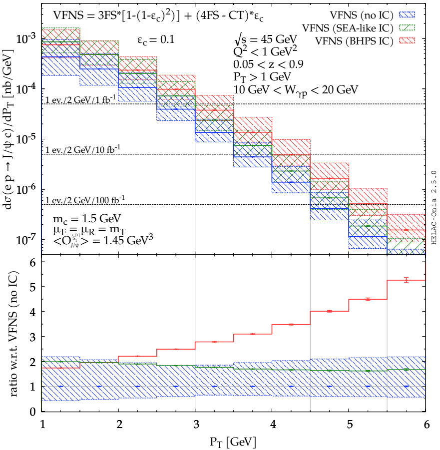

CF, J.-P. Lansberg, H.-S. Shao, Y. Yedelkina, PLB 811 (2020) 135926

- Same LO VFNS computation previously shown in green except for the charm-detection efficiency ε_c:

$$d\sigma^{\text{VFNS}} = d\sigma^{3\text{FS}}\left[1-(1-\varepsilon_c)^2\right] + \left(d\sigma^{4\text{FS}} - d\sigma^{\text{CT}}\right)\varepsilon_c$$

- At $\sqrt{s_{ep}} = 45$ GeV, yield limited to low P_T even with $\mathcal{L} = 100$ fb^{-1}
- But it is clearly observable if $\varepsilon_c = 0.1$ with $\mathcal{O}(500, 50, 5)$ events for $\mathcal{L} = (100, 10, 1)$ fb^{-1}
- At $\sqrt{s_{ep}} = 140$ GeV, P_T range up to 10 GeV with up to thousands of events with $\mathcal{L} = 100$ fb^{-1}
- Could be observed via charm jet

- 4FS $\gamma c \to J/\psi c$ depends on $c(x)$ and could be enhanced by intrinsic charm
- Small effect at $\sqrt{s_{ep}} = 140$ GeV [We used IC $c(x)$ encoded in CT14NNLO]
- Measurable effect at $\sqrt{s_{ep}} = 45$ GeV: BHPS valence-like peak visible!

Negative cross-sections at high energies

A. Colpani Serri, Y. Feng, CF, J.-P. Lansberg, M.A. Ozcelik, H.-S. Shao, Y. Yedelkina, PLB 835 (2022) 137556

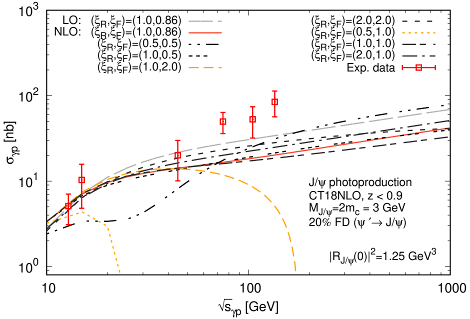

Experimental data:
H1 [M. Krämer, NPB 459 (1996) 3-50]
FTPS [B.H.Denby *et al.*, PRL 52 (1984) 795-798]
NA14 Coll. [R. Barate *et al.*, Z.Phys.C 33 (1987) 505]

Negative cross-sections at high energies

A. Colpani Serri, Y. Feng, CF, J.-P. Lansberg, M.A. Ozcelik, H.-S. Shao, Y. Yedelkina, PLB 835 (2022) 137556

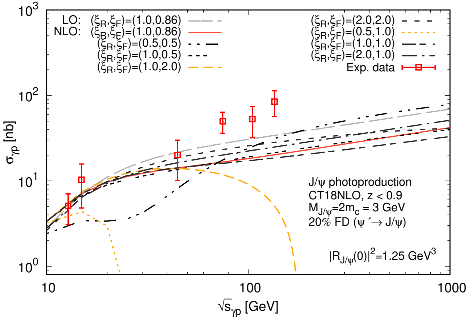

Experimental data:
H1 [M. Krämer, NPB 459 (1996) 3-50]
FTPS [B.H.Denby *et al.*, PRL 52 (1984) 795-798]
NA14 Coll. [R. Barate *et al.*, Z.Phys.C 33 (1987) 505]

- NLO cross section for J/ψ photoproduction becomes negative for large μ_F when $\sqrt{s_{\gamma p}}$ increases

Negative cross-sections at high energies

A. Colpani Serri, Y. Feng, CF, J.-P. Lansberg, M.A. Ozcelik, H.-S. Shao, Y. Yedelkina, PLB 835 (2022) 137556

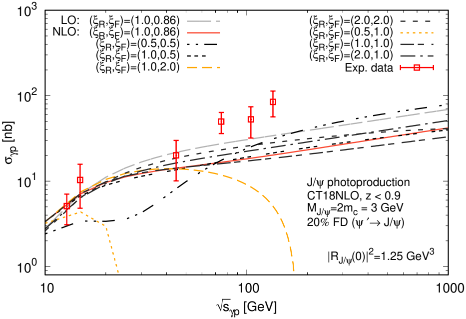

Experimental data:
H1 [M. Krämer, NPB 459 (1996) 3-50]
FTPS [B.H.Denby *et al.*, PRL 52 (1984) 795-798]
NA14 Coll. [R. Barate *et al.*, Z.Phys.C 33 (1987) 505]

- NLO cross section for J/ψ photoproduction becomes negative for large μ_F when $\sqrt{s_{\gamma p}}$ increases
- For $\mu_F = 2M_{\mathcal{Q}}$, $\sigma < 0$ as in case of η_c hadroproduction

J.-P. Lansberg, M.A. Ozcelik: EPJC 81 (2021) 6, 497

Negative cross-sections at high energies

A. Colpani Serri, Y. Feng, CF, J.-P. Lansberg, M.A. Ozcelik, H.-S. Shao, Y. Yedelkina, PLB 835 (2022) 137556

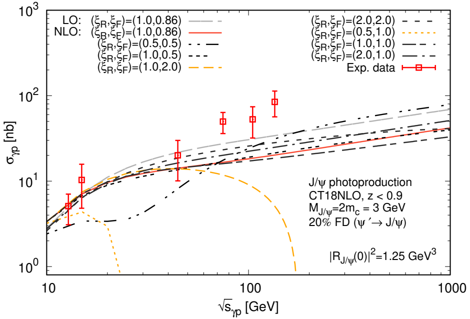

Experimental data:
H1 [M. Krämer, NPB 459 (1996) 3-50]
FTPS [B.H.Denby *et al.*, PRL 52 (1984) 795-798]
NA14 Coll. [R. Barate *et al.*, Z.Phys.C 33 (1987) 505]

- NLO cross section for J/ψ photoproduction becomes negative for large μ_F when $\sqrt{s_{\gamma p}}$ increases
- For $\mu_F = 2M_{\mathcal{Q}}$, $\sigma < 0$ as in case of η_c hadroproduction

J.-P. Lansberg, M.A. Ozcelik: EPJC 81 (2021) 6, 497

- 2 possible sources of negative partonic cross sections: loop corrections (interference) and from real emission (subtraction of IR poles)

Origin of negative cross-section values

A. Colpani Serri, Y. Feng, CF, J.-P. Lansberg, M.A. Ozcelik, H.-S. Shao, Y. Yedelkina, PLB 835 (2022) 137556

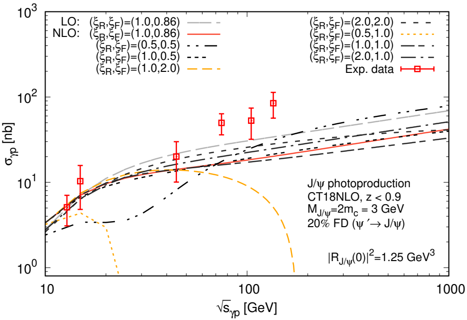

Experimental data:
H1 [M. Krämer, NPB 459 (1996) 3-50]
FTPS [B.H.Denby *et al.*, PRL 52 (1984) 795-798]
NA14 Coll. [R. Barate *et al.*, Z.Phys.C 33 (1987) 505]

- Initial state collinear divergences are removed via the subtraction into the PDFs via AP-CT

Origin of negative cross-section values

A. Colpani Serri, Y. Feng, CF, J.-P. Lansberg, M.A. Ozcelik, H.-S. Shao, Y. Yedelkina, PLB 835 (2022) 137556

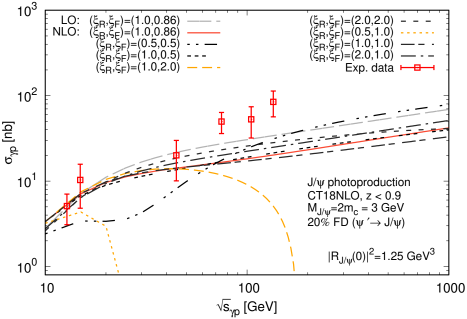

Experimental data:
H1 [M. Krämer, NPB 459 (1996) 3-50]
FTPS [B.H.Denby *et al.*, PRL 52 (1984) 795-798]
NA14 Coll. [R. Barate *et al.*, Z.Phys.C 33 (1987) 505]

- Initial state collinear divergences are removed via the subtraction into the PDFs via AP-CT
- $\hat{s} \to \infty : \ \hat{\sigma}^{NLO}_{\gamma i} \propto \alpha_s(\mu_R) \left(\bar{c}_1^{(\gamma i)} \log \frac{M_Q^2}{\mu_F{}^2} + c_1^{(\gamma i)} \right), A_{\gamma i} = \frac{c_1^{(\gamma i)}}{\bar{c}_1^{(\gamma i)}}, \boxed{A_{\gamma g} = A_{\gamma q}}$

A scale prescription for μ_F

J.-P. Lansberg, M.A. Ozcelik: EPJC 81 (2021) 6, 497

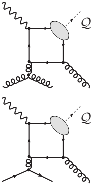

- In principle, such negative terms should be compensated by the evolution of the PDFs governed by the DGLAP equations;

A scale prescription for μ_F

J.-P. Lansberg, M.A. Ozcelik: EPJC 81 (2021) 6, 497

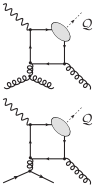

- In principle, such negative terms should be compensated by the evolution of the PDFs governed by the DGLAP equations;
- $A_{\gamma g}, A_{\gamma q}$ are process-dependent, while the DGLAP equations are process-independent, which makes the compensation imperfect;

A scale prescription for μ_F

J.-P. Lansberg, M.A. Ozcelik: EPJC 81 (2021) 6, 497

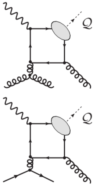

- In principle, such negative terms should be compensated by the evolution of the PDFs governed by the DGLAP equations;
- $A_{\gamma g}, A_{\gamma q}$ are process-dependent, while the DGLAP equations are process-independent, which makes the compensation imperfect;
- But as $A_{\gamma g} = A_{\gamma q}$, we can choose μ_F such that $\lim_{\hat{s}\to\infty} \hat{\sigma}_{\gamma i}^{NLO} = 0$

A scale prescription for μ_F

J.-P. Lansberg, M.A. Ozcelik: EPJC 81 (2021) 6, 497

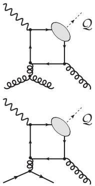

- In principle, such negative terms should be compensated by the evolution of the PDFs governed by the DGLAP equations;
- $A_{\gamma g}, A_{\gamma q}$ are process-dependent, while the DGLAP equations are process-independent, which makes the compensation imperfect;
- But as $A_{\gamma g} = A_{\gamma q}$, we can choose μ_F such that $\lim_{\hat{s}\to\infty} \hat{\sigma}^{NLO}_{\gamma i} = 0$
- This amounts to consider that all the QCD corrections are in the PDFs

A scale prescription for μ_F

J.-P. Lansberg, M.A. Ozcelik: EPJC 81 (2021) 6, 497

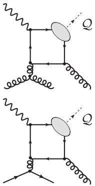

- In principle, such negative terms should be compensated by the evolution of the PDFs governed by the DGLAP equations;
- $A_{\gamma g}, A_{\gamma q}$ are process-dependent, while the DGLAP equations are process-independent, which makes the compensation imperfect;
- But as $A_{\gamma g} = A_{\gamma q}$, we can choose μ_F such that $\lim_{\hat{s}\to\infty} \hat{\sigma}^{NLO}_{\gamma i} = 0$
- This amounts to consider that all the QCD corrections are in the PDFs
- The choice of factorisation scale to avoid possible negative hadronic cross-section: $\mu_F = \hat{\mu}_F = M_{\mathcal{Q}} e^{A_{\gamma i}/2}$;

A scale prescription for μ_F

J.-P. Lansberg, M.A. Ozcelik: EPJC 81 (2021) 6, 497

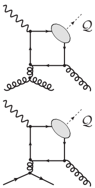

- In principle, such negative terms should be compensated by the evolution of the PDFs governed by the DGLAP equations;
- $A_{\gamma g}, A_{\gamma q}$ are process-dependent, while the DGLAP equations are process-independent, which makes the compensation imperfect;
- But as $A_{\gamma g} = A_{\gamma q}$, we can choose μ_F such that $\lim_{\hat{s}\to\infty} \hat{\sigma}^{NLO}_{\gamma i} = 0$
- This amounts to consider that all the QCD corrections are in the PDFs
- The choice of factorisation scale to avoid possible negative hadronic cross-section: $\mu_F = \hat{\mu}_F = M_{\mathcal{Q}} e^{A_{\gamma i}/2}$;
- For J/ψ (Υ) photoproduction: $\hat{\mu}_F = 0.86 M_{\mathcal{Q}}$ $(P_T \in [0, \infty],\ z < 0.9)$

Results with $\hat{\mu}_F = 0.86M$

A. Colpani Serri, Y. Feng, CF, J.-P. Lansberg, M.A. Ozcelik, H.-S. Shao, Y. Yedelkina, PLB835 (2022) 137556

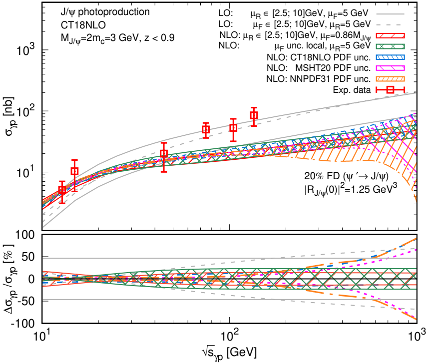

Exp. data: H1 [M. Krämer, NPB 459 (1996) 3-50]; FTPS [B.H.Denby *et al.*, PRL 52 (1984) 795-798]; NA14 Coll. [R. Barate *et al.*, Z.Phys.C 33 (1987) 505]

- PDF uncertainties increase at large $\sqrt{s}$ (i.e. small x)
- The μ_R unc. are reduced at NLO in comparison with LO

Results with $\hat{\mu}_F = 0.86M$

A. Colpani Serri, Y. Feng, CF, J.-P. Lansberg, M.A. Ozcelik, H.-S. Shao, Y. Yedelkina, PLB835 (2022) 137556

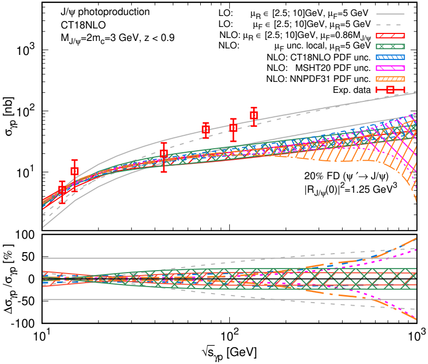

Exp. data: H1 [M. Krämer, NPB 459 (1996) 3-50]; FTPS [B.H.Denby *et al.*, PRL 52 (1984) 795-798]; NA14 Coll. [R. Barate *et al.*, Z.Phys.C 33 (1987) 505]

- PDF uncertainties increase at large $\sqrt{s}$ (i.e. small x)
- The μ_R unc. are reduced at NLO in comparison with LO
- Increase of μ_R unc. from $\sqrt{s_{\gamma p}} \gtrsim 50$ GeV from the loop corr.
- At NNLO we expect a further reduction of μ_R uncertainties

P_T-differential cross sections at NLO

A. Colpani Serri, Y. Feng, CF, J.-P. Lansberg, M.A. Ozcelik, H.-S. Shao, Y. Yedelkina, PLB835 (2022) 137556

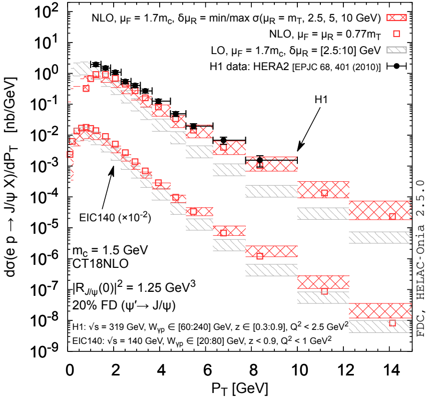

- for P_T-dependent cross-sections:
  $\lim_{\hat{s}\to\infty} c_1^{(\gamma i)}(p_T)/\bar{c}_1^{(\gamma i)}(p_T) \propto (P_T/M_{\mathcal{Q}})^2$
  $\Rightarrow \hat{\mu}_F = M_{\mathcal{Q}} e^{c_{\gamma i}^{(1)}/2\bar{c}_{\gamma i}^{(1)}} \propto M_{\mathcal{Q}} e^{P_T^2/M_{\mathcal{Q}}^2}$
- Common dynamical scale choice: $\mu_F = (0.5, 1, 2) m_T$
- one can use $\mu_F = \alpha\sqrt{M_{\mathcal{Q}}^2 + P_T^2}$ or $\mu_F = \sqrt{(\beta M_{\mathcal{Q}})^2 + P_T^2}$
- if P_T is large, then $\mu_F \propto P_T$

- For $\mu_F = \hat{\mu}_F$ with $< P_T^2 >= 2.5\text{GeV}^2$ (for J/ψ at HERA energies), we get $\alpha = 0.77$ and $\beta = 0.7$
- All choices give similar results, compatible with the latest H1 data
- NLO* predictions for the EIC at 140 GeV compatible with full NLO

$\sigma_{ep}(\sqrt{s})$

A. Colpani Serri, Y. Feng, CF, J.-P. Lansberg, M.A. Ozcelik, H.-S. Shao, Y. Yedelkina, PLB835 (2022) 137556

Exp.	$\sqrt{s_{ep}}$	$\mathcal{L}$ (fb^{-1})	$N_{J/\psi}$	$N_{\Upsilon(1S)}$
EicC	16.7	100	$1.5^{+0.3}_{-0.2} \cdot 10^6$	$2.3^{+1.1}_{-1.4} \cdot 10^0$
AMBER	17.3	1	$1.6^{+0.3}_{-0.3} \cdot 10^4$	< 1
EIC	45	100	$8.5^{+0.5}_{-1.0} \cdot 10^6$	$6.1^{+0.7}_{-0.8} \cdot 10^2$
EIC	140	100	$2.5^{+0.1}_{-0.4} \cdot 10^7$	$7.6^{+0.3}_{-0.7} \cdot 10^3$
LheC	1183	100	$9.3^{+2.9}_{-2.9} \cdot 10^7$	$8.1^{+0.4}_{-0.7} \cdot 10^4$
FCC-eh	3464	100	$1.6^{+0.2}_{-1.0} \cdot 10^8$	$1.8^{+0.1}_{-0.2} \cdot 10^5$

We expect μ_R unc. to shrink at NNLO:
Possibility to constrain PDF with differential measurements

Rem. $N_{\psi'} \simeq 0.08 \times N_{J/\psi}$, $N_{\Upsilon(2S)} \simeq 0.4 \times N_{\Upsilon(1S)}$, $N_{\Upsilon(3S)} \simeq 0.35 \times N_{\Upsilon(1S)}$

Conclusions

- The CSM up to $\alpha\alpha_s^3$ reproduces photoproduction at HERA up to scale-uncertainty

  Agreement improved when accounting for J/ψ+charm and $b \to J/\psi$ FD

Conclusions

- The CSM up to $\alpha\alpha_s^3$ reproduces photoproduction at HERA up to scale-uncertainty

  Agreement improved when accounting for J/ψ+charm and $b \to J/\psi$ FD

- The estimations for EIC can rely on CSM only

Conclusions

- The CSM up to $\alpha\alpha_s^3$ reproduces photoproduction at HERA up to scale-uncertainty

  Agreement improved when accounting for J/ψ+charm and $b \to J/\psi$ FD

- The estimations for EIC can rely on CSM only

- NLO QCD corrections are important for P_T-integrated σ

Conclusions

- The CSM up to $\alpha\alpha_s^3$ reproduces photoproduction at HERA up to scale-uncertainty

  Agreement improved when accounting for J/ψ+charm and $b \to J/\psi$ FD

- The estimations for EIC can rely on CSM only

- NLO QCD corrections are important for P_T-integrated σ

- A specific μ_F choice can be employed to avoid a possible over subtraction of collinear divergences which lead to negative NLO σ values at large $\sqrt{s_{\gamma p}}$

Conclusions

- The CSM up to $\alpha\alpha_S^3$ reproduces photoproduction at HERA up to scale-uncertainty

  Agreement improved when accounting for J/ψ+charm and $b \to J/\psi$ FD
- The estimations for EIC can rely on CSM only
- NLO QCD corrections are important for P_T-integrated σ
- A specific μ_F choice can be employed to avoid a possible over subtraction of collinear divergences which lead to negative NLO σ values at large $\sqrt{s_{\gamma p}}$
- Loop corrections matter and significant NNLO corrections (likely positive) are expected as well as a further reduction of the μ_R unc., esp. around 100 GeV

Conclusions

- The CSM up to $\alpha\alpha_s^3$ reproduces photoproduction at HERA up to scale-uncertainty

  Agreement improved when accounting for J/ψ+charm and $b \to J/\psi$ FD

- The estimations for EIC can rely on CSM only

- NLO QCD corrections are important for P_T-integrated σ

- A specific μ_F choice can be employed to avoid a possible over subtraction of collinear divergences which lead to negative NLO σ values at large $\sqrt{s_{\gamma p}}$

- Loop corrections matter and significant NNLO corrections (likely positive) are expected as well as a further reduction of the μ_R unc., esp. around 100 GeV

- This would likely allow one to better probe gluon PDFs at small-x and $\mu_F \sim M$.

Conclusions

- The CSM up to $\alpha\alpha_s^3$ reproduces photoproduction at HERA up to scale-uncertainty
  Agreement improved when accounting for J/ψ+charm and $b \to J/\psi$ FD
- The estimations for EIC can rely on CSM only
- NLO QCD corrections are important for P_T-integrated σ
- A specific μ_F choice can be employed to avoid a possible over subtraction of collinear divergences which lead to negative NLO σ values at large $\sqrt{s_{\gamma p}}$
- Loop corrections matter and significant NNLO corrections (likely positive) are expected as well as a further reduction of the μ_R unc., esp. around 100 GeV
- This would likely allow one to better probe gluon PDFs at small-x and $\mu_F \sim M$.

Thank you

Backup

Kinematics and cross section

CF, J.-P. Lansberg, H.-S. Shao, Y. Yedelkina, PLB 811 (2020) 135926

- $s_{ep} = (P_e + P_p)^2 = 4E_eE_p$; $s_{\gamma p} = W^2_{\gamma p} = (P_\gamma + P_p)^2$; $P_\gamma = x_\gamma P_e$, so $s_{\gamma p} = x_\gamma s_{ep}$
- $z = \frac{P_{\mathcal{Q}}\cdot P_p}{P_\gamma \cdot P_p}$: fraction of the photon energy taken by the J/ψ in the proton rest frame
- cross section:

$$\frac{d\sigma}{dz dP_T} = \int_{x_\gamma^{\min}}^{1} dx_\gamma \frac{2x_a P_T f_{\gamma/e}(x_\gamma, Q^2_{\max}) f_{a/p}(x_a(x_\gamma), \mu_F)}{z(1-z)} \times \frac{1}{16\pi \hat{s}^2} \overline{|\mathcal{M}(\gamma + a \to \mathcal{Q} + k)|^2},$$

where $x_a = \frac{M_T^2 - m^2_{\mathcal{Q}} z}{x_\gamma s_{ep} z(1-z)}$ and $x_\gamma^{\min} = \frac{M_T^2 - m^2_{\mathcal{Q}} z}{s_{ep} z(1-z)}$

- WW distribution

$$f_{\gamma/e}(x_\gamma, Q^2_{\max}) = \frac{\alpha}{2\pi}\left[\frac{1+(1-x_\gamma)^2}{x_\gamma} \ln \frac{Q^2_{\max}}{Q^2_{\min}(x_\gamma)} + 2m_e^2 x_\gamma \left(\frac{1}{Q^2_{\max}} - \frac{1}{Q^2_{\min}(x_\gamma)}\right)\right]$$

where $Q^2_{\min}(x_\gamma) = m_e^2 x_\gamma^2/(1-x_\gamma)$

VFNS treatment of J/ψ+charm yield

CF, J.-P. Lansberg, H.-S. Shao, Y. Yedelkina, PLB 811 (2020) 135926

J/ψ+charm production follows from

- $\gamma + g \to J/\psi + c + \bar{c}$ @ $\alpha\alpha_s^3$ (3FS)
- $\gamma + \{c, \bar{c}\} \to J/\psi + \{c, \bar{c}\}$ @ $\alpha\alpha_s^2$ (4FS)

$$d\sigma_{\gamma c \to J/\psi + c} = \frac{1}{2\left(\hat{s} - m_c^2\right)} dx_c\, f_{c/p}(x_c, \mu_F^2) \times \overline{\left|\mathcal{M}_{\gamma c \to J/\psi c}\right|^2} d\Phi(p_\gamma, p_c \to P_\mathcal{Q}, p_c'),$$

with

$$f_{c/p}(x_c, \mu_F^2) = \tilde{f}_{c/p}^{(1)}(x_c, \mu_F^2) + \mathcal{O}(\alpha_s^2),$$

where

$$\tilde{f}_{c/p}^{(1)}(x_c, \mu_F^2) = \frac{\alpha_s}{2\pi} \log\left(\frac{\mu_F^2}{m_c^2}\right) \int_{x_c}^1 \frac{dz}{z} P_{qg}(z) f_{g/p}\left(\frac{x_c}{z}, \mu_F^2\right)$$

with AP splitting function $P_{qg}(z) = \frac{1}{2}\left[z^2 + (1-z)^2\right]$. Overlap CT to be subtracted from 3FS:

$$d\sigma_{\mathrm{CT}, \gamma c \to J/\psi + c} = \frac{1}{2\left(\hat{s} - m_c^2\right)} dx_c\, \tilde{f}_{c/p}^{(1)}(x_c, \mu_F^2) \overline{\left|\mathcal{M}_{\gamma c \to J/\psi c}\right|^2} d\Phi(p_\gamma, p_c \to P_\mathcal{Q}, p_c').$$

$b \to J/\psi$ feed-down

CF, J.-P. Lansberg, H.-S. Shao, Y. Yedelkina, PLB 811 (2020) 135926

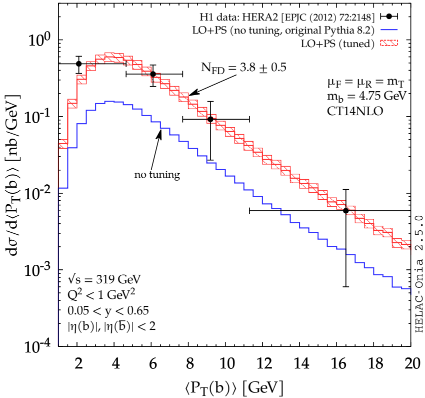

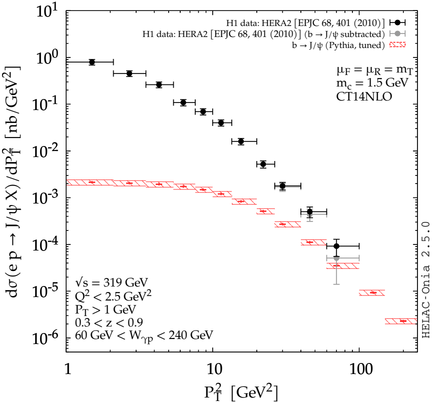

H1 $b\bar{b}$ production from **EPJC 72 (2012) 2148** [Note: $\langle P_T(b)\rangle = \sqrt{(P^2_{T,b} + P^2_{T,\bar{b}})/2}$]

N_{FD} = 3.8 $\pm$ 0.5 estimated via χ^2−minimisation

$b \to J/\psi$ tuned with PYTHIA 8.2

General structure of NLO corrections

M. Krämer, NPB 459, 3 (1996)

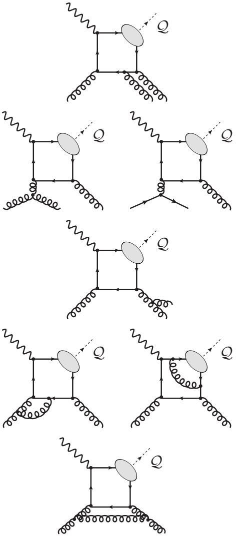

Singularities at NLO [and how they are removed]:

- Real emission
  - Infrared divergences: Soft [cancelled by loop IR contr.]
  - Infrared divergences: Collinear
    - initial state [subtracted via “renormalisation” of collinear PDFs (Altarelli-Parisi counter-terms)]
    - final state [cancelled by loop IR contr.]
- Virtual (loop) contribution
  - Ultraviolet divergences: [removed by renormalisation]
  - Infrared divergences: [cancelled by real Infrared contribution]
- We use the **FDC** code to produce NLO results

[J.-X. Wang Nucl.Instrum.Meth. A534(2004)241-245]

[The quark and antiquark attached to the blob are taken as on-shell and their relative velocity *v* is set to zero.]

Scale uncertainty for a fixed scale

A. Colpani Serri, Y. Feng, CF, J.-P. Lansberg, M.A. Ozcelik, H.-S. Shao, Y. Yedelkina, PLB835 (2022) 137556

- scale uncertainties are usually evaluated as

$$\Delta\sigma(\mu) = \frac{|\sigma(2\mu) - \sigma(\mu/2)|}{2}$$

- wider variations necessarily lead to wider uncertainties
- we used the following rescaling

$$\Delta_\xi\sigma(\mu) = \left| \frac{\sigma(\xi\mu) - \sigma(\mu/\xi)}{2} \frac{\ln 2}{\ln \xi} \right|$$

- one can then consider a *local* uncertainty, connected to $\frac{\partial\sigma}{\partial \log \mu}$ as:

$$\lim_{\xi \to 1} \Delta_\xi \sigma = \ln 2 \times \left| \frac{\partial \sigma(\mu)}{\partial \ln \mu} \right|$$